

Fermi surface and pseudogap in highly doped Sr₂IrO₄

Y. Alexanian,^{1,*} A. de la Torre,² S. McKweon Walker,³ M. Straub,¹ G. Gatti,¹ A. Hunter,¹ S. Mandloi,¹ E. Cappelli,¹ S. Riccò,¹ F. Y. Bruno,⁴ M. Radovic,⁵ N. C. Plumb,⁵ M. Shi,⁵ J. Osiecki,⁶ C. Polley,⁶ T. K. Kim,⁷ P. Dudin,^{7,8} M. Hoesch,⁹ R. S. Perry,^{10,11} A. Tamai,¹ and F. Baumberger^{1,5}

¹*Department of Quantum Matter Physics, University of Geneva,
24 Quai Ernest-Ansermet, CH-1211, Geneva, Switzerland*

²*Department of Physics, Brown University, Providence, Rhode Island 02912, USA*

³*Laboratory of Advanced Technology, University of Geneva,
24 Quai Ernest-Ansermet, CH-1211, Geneva, Switzerland*

⁴*GFMC, Departamento de Física de Materiales, Universidad Complutense de Madrid, 28040 Madrid, Spain*

⁵*Swiss Light Source, Paul Scherrer Institut, CH-5232 Villigen PSI, Switzerland*

⁶*MAX IV Laboratory, Lund University, SE-211 00 Lund, Sweden*

⁷*Diamond Light Source, Harwell Campus, Didcot, OX11 0DE, United Kingdom*

⁸*Synchrotron SOLEIL, L'Orme des Merisiers, Saint Aubin-BP 48, 91192 Gif sur Yvette Cedex, France*

⁹*Deutsches Elektronen-Synchrotron DESY, Notkestraße 85, 22607 Hamburg, Germany*

¹⁰*ISIS Pulsed Neutron and Muon Source, STFC Rutherford Appleton Laboratory,
Harwell Campus, Didcot, Oxon OX11 0QX, United Kingdom*

¹¹*London Centre for Nanotechnology and Department of Physics and Astronomy,
University College London, London WC1E 6BT, United Kingdom*

(Dated: November 28, 2024)

The fate of the Fermi surface in bulk electron-doped Sr₂IrO₄ remains elusive, as does the origin and extension of its pseudogap phase. Here, we use high-resolution angle-resolved photoelectron spectroscopy (ARPES) to investigate the electronic structure of Sr_{2-x}La_xIrO₄ up to $x = 0.2$, a factor of two higher than in previous work. Our findings reveal that the Fermi surface evolves smoothly with doping. Notably, the antinodal pseudogap persists up to the highest doping level, while nodal quasiparticle coherence increases monotonously. This demonstrates that the sharp increase in Hall carrier density recently observed above $x^* = 0.16$ [1] cannot be attributed to the closure of the pseudogap. Further, we determine a temperature boundary of the pseudogap of $T^* \simeq 200$ K for $x = 0.2$, comparable to cuprates. Our results suggest that pseudogaps are a generic feature of doped quasi-2D antiferromagnetic Mott insulators, likely related to short range magnetic correlations.

The pseudogap (PG) in hole doped cuprates is one of the most enigmatic properties of correlated electron systems. ARPES experiments established that the cuprate PG is anisotropic and selectively suppresses the low-energy spectral weight near $(\pi, 0)$, leaving apparent Fermi arcs extending out from the node along the Brillouin zone diagonal [2, 3]. However, the origin of the PG and its relation with the rich phase diagram of cuprates remain controversial, not least because there is little thermodynamic evidence for a genuine phase transition at the critical doping p^* and temperature T^* where the PG closes [4–7]. When superconductivity is suppressed in high magnetic fields, several cuprate families show a strong peak in the electronic specific heat near p^* , in some cases accompanied by a $\log(1/T)$ dependence at low temperatures. Around the same doping level, the Hall carrier density increases from the doping p to $1 + p$ [8, 9]. Whether these signatures are caused by a quantum critical point associated with the closure of the PG remains debated.

The recent observation by Hsu *et al.* of similar anomalies in the electronic specific heat and Hall density in the electron doped iridate Sr_{2-x}La_xIrO₄ provides complementary insight into these open questions [1]. Undoped Sr₂IrO₄ is a single band antiferromagnetic (AF) insulator, commonly described as a pseudospin $J_{\text{eff}} = 1/2$

Mott state [10–12], although other interpretations have been put forward [13]. ARPES experiments at low La doping revealed a PG with the same anisotropy in momentum space known from cuprates [14–16]. Crucially though, Sr_{2-x}La_xIrO₄ shows no signs of superconductivity up to the highest doping of $x = 0.2$ investigated so far [17]. Thus, the PG state in iridates does not promote superconductivity. Neither does it appear to be caused by preformed pairs. On the other hand, short range AF spin correlations in Sr_{2-x}La_xIrO₄ closely reflect spin excitations in cuprates [18–21], although no charge or spin orders were found in iridates. These observations prompted suggestions that the PG in iridates is driven by magnetic fluctuations [1, 14].

Hsu *et al.* interpreted the anomalies in specific heat and Hall density as a signature of the closure of the PG at a critical La doping $x^* \simeq 0.16$ [1]. This is qualitatively consistent with an ARPES study of K surface doped Sr₂IrO₄ that found a transition from a pseudogapped regime to a conventional large Fermi surface (FS) around a K coverage of ~ 0.85 monolayer (ML) [22]. However, it is unclear whether such a metal/AF-insulator interface is representative of highly bulk doped samples, which are metallic and paramagnetic. In bulk electron doped samples there is thus far no direct evidence for a closure of the PG.

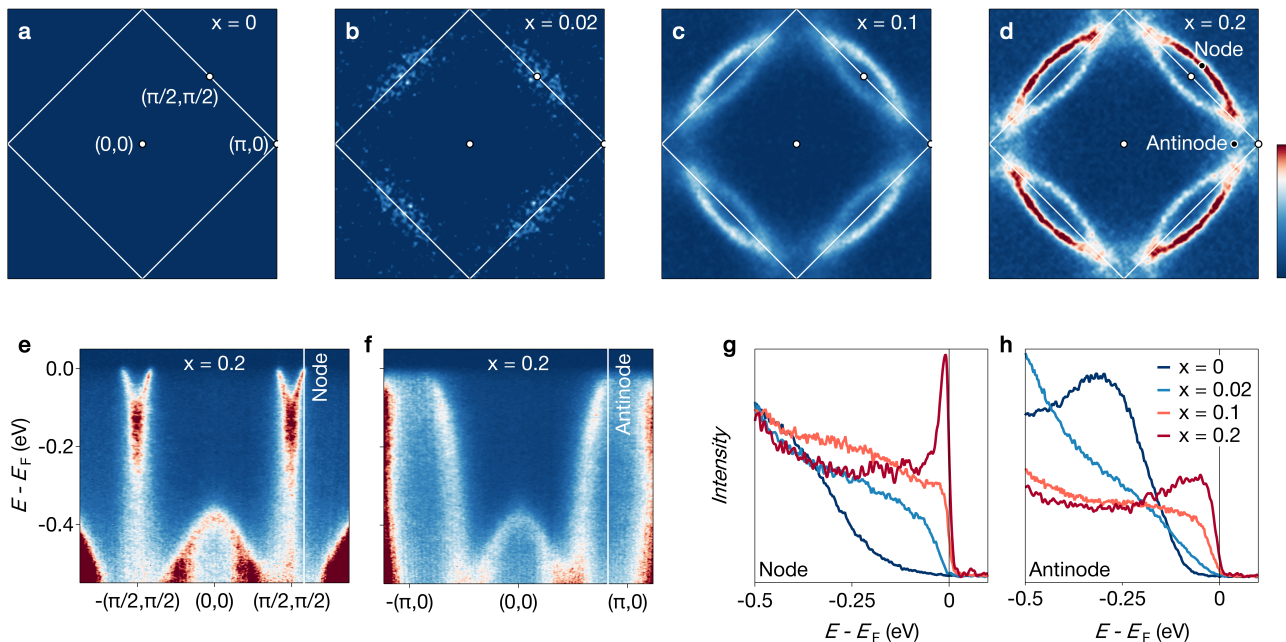


FIG. 1. **Collapse of the spin-orbit driven Mott insulating ground state and emergence of the pseudogap state in $\text{Sr}_{2-x}\text{La}_x\text{IrO}_4$.** **a-d** Fermi surfaces for $x = 0$, $x = 0.02$, $x = 0.1$, and $x = 0.2$, respectively. Data were measured at $T \simeq 50$ K (**a,b**) and $T \simeq 10$ K (**c,d**) with a photon energy $h\nu = 100$ eV and have been fourfold rotationally averaged. **e,f** ARPES band dispersion of $\text{Sr}_{1.8}\text{La}_{0.2}\text{IrO}_4$ along the nodal $(0,0) - (\pi,\pi)$ and antinodal $(0,0) - (\pi,0)$ directions, illustrating the nodal-antinodal dichotomy. **g,h** Doping dependence of energy distribution curves (EDCs) at the nodal and antinodal positions indicated in **d-f**.

Here, we report high-resolution ARPES data from the same batch of $\text{Sr}_{2-x}\text{La}_x\text{IrO}_4$ samples studied by Hsu *et al.* [1]. We find that the electronic structure evolves smoothly across x^* . Quasiparticle coherence increases monotonously with doping while the nodal Fermi velocity is largely constant. Most importantly, the PG remains open up to at least $x = 0.2$. This demonstrates that the crossover at x^* neither arises from the pseudogap closure nor from an enhanced mass of nodal quasiparticles. We further show that for $x = 0.2$, the PG closes around $T^* = 200$ K, comparable to T^* of cuprates and to the Néel transition temperature of the undoped compounds.

Fig. 1 illustrates the doping dependence of the electronic structure of $\text{Sr}_{2-x}\text{La}_x\text{IrO}_4$ from the pristine compound to $x = 0.2$. Incoherent spectral weight at the Fermi energy E_F first appears at $x = 0.02$. However, a defined PG state with coherent Fermi arcs stretching from the nodal $(0,0) - (\pi/2, \pi/2)$ direction and evolving into incoherent antinodal excitations only emerges at $x = 0.1$. The transition from an insulating to a pseudogapped state and the persistence of the nodal-antinodal dichotomy up to $x = 0.2$ are evident from the Energy Distribution Curves (EDCs) in Fig. 1(g,h). EDCs at the antinode show that although spectral weight shifts closer to E_F with increasing doping, a gap persists across the entire doping range. In contrast, nodal EDCs display the Fermi-Dirac cutoff of ungapped excitations for $x = 0.1$ and $x = 0.2$. No-

tably, the quasiparticle peak – nearly absent for $x = 0.1$ – becomes well-defined at $x = 0.2$. This is a signature of a striking increase of the nodal quasiparticle coherence with doping. These ARPES signatures of the PG state of Sr_2IrO_4 are highly reminiscent of cuprates. Yet there are two key differences. First, the FS in Sr_2IrO_4 is electron-like and centered at $(0,0)$, contrasting with the hole-like FS at (π,π) of the cuprates. Second, a doubling of the in-plane unit cell arising from a rotation of the oxygen octahedra causes a back folding of the FS in $\text{Sr}_{2-x}\text{La}_x\text{IrO}_4$ [14, 23, 24].

Our data reveal that electron-doped $\text{Sr}_{2-x}\text{La}_x\text{IrO}_4$ remains in a pseudogapped state up to $x = 0.2$. Notably, the emergence of a distinct coherent nodal quasiparticle peak from the broad incoherent features dominating the spectra at half-filling is also a key feature of pseudogapped cuprates. There, it appears at doping levels deep into the superconducting state but below the critical doping where the PG closes [25, 26]. This indicates that our highly doped iridates are approaching the pseudogap doping boundary, and that further doping could lead to the predicted ungapped but still nodal-antinodal differentiated state [27]. It further highlights the lack of a superconductivity dome throughout the iridate pseudogap phase. The physical origin of the iridate PG is thus likely unrelated to superconductivity.

Fig. 2 quantifies the evolution of the electronic struc-

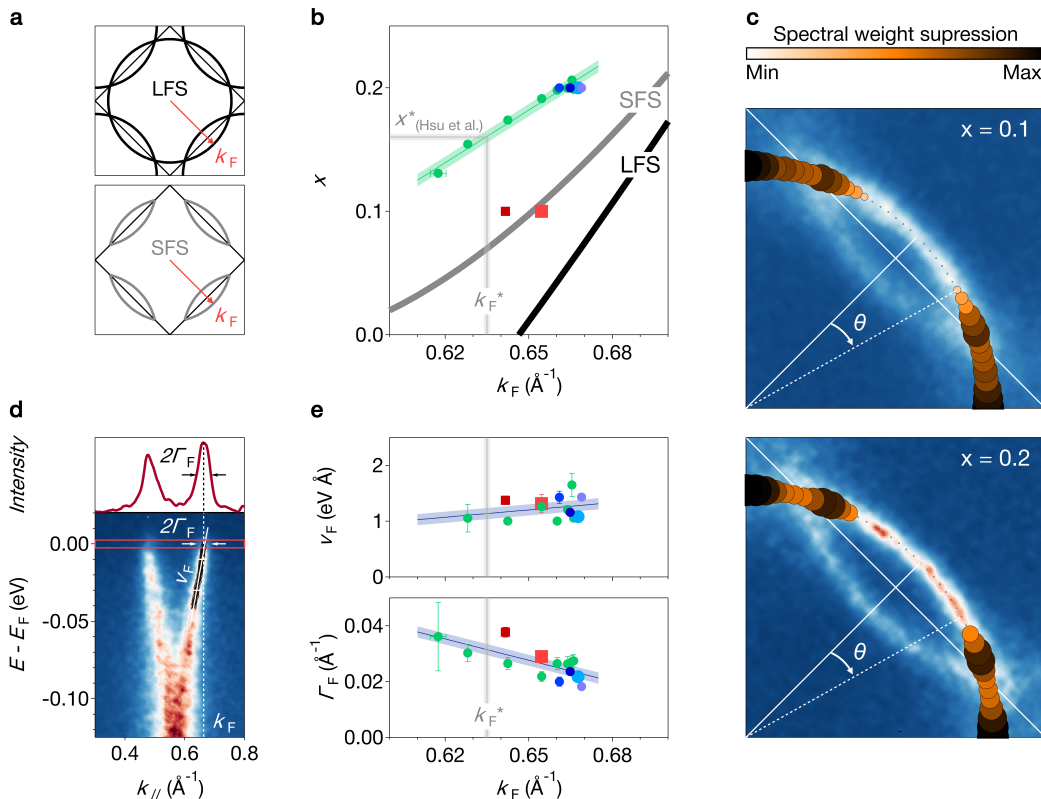


FIG. 2. Continuous evolution of the electronic structure of $\text{Sr}_{2-x}\text{La}_x\text{IrO}_4$ with doping. **a** Schematic representation of the large (LFS) and small (SFS) Fermi surface scenarios. **b** Lanthanum concentration x versus Fermi momentum k_F . The green markers represent experimental data measured on a single sample which showed a smooth spatial variation of the La doping (see Supplementary Information A). A linear fit of these data (green line) defines the critical Fermi momentum k_F^* corresponding to the critical chemical doping x^* of Ref. [1] (light grey line). k_F measurements on other samples are represented by different colored markers - squares for lightly doped (LD) and blue circles for highly doped (HD) samples. The thick black and grey lines illustrate the relationship between x and k_F in the large and small FS scenarios, respectively. **c** Spectral weight suppression in the PG (markers) overlaid on a quadrant of the Fermi surface. **d** Experimental definition of Fermi momentum k_F , Fermi velocity v_F , and scattering rate at the Fermi energy Γ_F . See methods for details. **e** Fermi velocity v_F (top) and scattering rate at the Fermi energy Γ_F (bottom) as a function of the Fermi momentum k_F . Shaded lines are linear fits of the experimental data.

ture of $\text{Sr}_{2-x}\text{La}_x\text{IrO}_4$ between $x = 0.1$ and $x = 0.2$. To this end, we measured several samples grown with two different procedures (see Methods): lightly doped (nominal doping $x = 0.1$) and highly doped (nominal doping $x = 0.2$) samples, referred to as LD and HD, respectively. Crucially, our HD samples come from the same batch as those measured by Hsu *et al.* [1], allowing for a straightforward comparison of results. We determined the precise La content x in both sets with energy-dispersive x-ray spectroscopy (EDX). These measurements revealed a slow variation in x near the edges of some HD samples which we exploit to obtain a smooth doping dependence from spatially resolved μ -spot ARPES measurements (see Supplementary Information A).

Hsu *et al.* interpret the Hall carrier density crossover

from $n_H = 1 + x$ at high doping to $n_H = x$ at low doping as a reconstruction of a conventional large FS (LFS) upon entering the PG phase. An ungapped LFS – illustrated in Fig. 2a – has a well defined relation of Fermi wave vector k_F and carrier density per Ir defined by the Luttinger theorem and shown as a black line in Fig. 2b. Here, we identify the carrier density per Ir with the La concentration x which is the case if the additional electron of La dopants fully delocalizes. A simplified scenario for the PG phase is a small FS (SFS) consisting only of the lens-like nodal electron pockets while the antinodal hole pockets are gapped. The corresponding relation of k_F and x is shown as grey line in Fig. 2b. Clearly, the experimental data from HD samples do not align with either scenario. Notably though, HD samples show a lin-

ear evolution of k_F with x , without any discontinuity at $x^* \simeq 0.16$. This confirms that x^* does not correspond to a qualitative change in the FS. It further allows a precise quantification of the nodal k_F^* corresponding to the critical doping x^* .

The deviation of the experimental k_F values from the simple LFS/SFS scenarios can arise from different effects. In Fig. 2c we quantify the spectral weight suppression in the PG state along the FS (see Supplementary Information B for details). This shows an extended ungapped region stretching out from the nodal point up to $\theta \approx 13.5^\circ$ for $x = 0.1$ and $\theta \approx 18^\circ$ for $x = 0.2$, slightly larger than observed in overdoped $\text{Bi}_2\text{Sr}_2\text{CaCu}_2\text{O}_{8+\delta}$ [28]. Importantly though, the PG sets on deep into the nodal lens pockets for both $x = 0.1$ (LD sample) and $x = 0.2$ (HD sample). Hence, a conventional closed Fermi surface does not emerge up to the highest doping of $x = 0.2$, which questions the applicability of the Luttinger theorem. Fig. 2b further reveals that LD and HD samples show a distinct $k_F(x)$ relation implying that in one or both cases, the itinerant carrier density differs from the La concentration. This can arise from a partial localization of doped electrons, as it is observed for instance in SrTiO_3 2D electron gases [29]. A plausible alternative is co-doping from a slightly off-stoichiometric oxygen content. Because of these complexities, k_F is a more reliable indicator of the electronic state than the La concentration.

In Fig. 2e we quantify the doping evolution of the Fermi velocity v_F and the scattering rate at the Fermi energy Γ_F , both defined experimentally in Fig. 2d (see Methods for details). Plotting these quantities as a function of k_F shows no significant difference between LD and HD samples, confirming that k_F is a robust indicator of the actual electronic state. As the effective electron doping increases, we only observe a small gradual increase in v_F , with no abrupt changes detected around k_F^* . The reduction of the scattering rate with increasing k_F is more pronounced, in line with the significant rise in nodal quasiparticle coherence observed between $x = 0.1$ and $x = 0.2$ in Fig. 1. Importantly though, no discontinuity is observed in either quantity at the critical doping x^* .

Hsu *et al.* reported a strong enhancement of the electronic specific heat coefficient γ of $\text{Sr}_{2-x}\text{La}_x\text{IrO}_4$ over an extended doping range of $x \simeq 0.12 - 0.17$. They further point out that their data show no signs of a logarithmic divergence of the specific heat, typical for quantum critical systems [1]. In a conventional quasi-2D metal, $\gamma \propto m^* \propto 1/v_F$ where m^* is the quasiparticle effective mass. An enhancement of γ thus corresponds to an enhanced effective mass m^* and a correspondingly reduced Fermi velocity v_F . Our data are difficult to reconcile with such an interpretation of the measured electronic specific heat. Specifically, Fig. 2e shows that the nodal Fermi velocity remains nearly constant from $x^* \simeq 0.16$ up to the highest doping of $x = 0.2$. In contrast Hsu *et al.* report

a roughly 6-fold change of γ over the same doping range. Our direct measurements of the Fermi surface further exclude a Lifshitz transition and associated divergence in the single particle density of states in the relevant doping range. Moreover, we find that the low-energy spectral weight near $(\pi, 0)$ is almost fully suppressed suggesting that these states – which may be more strongly renormalized – should not contribute to the electronic specific heat.

Our data show that the PG shrinks with increasing doping but persists up to at least $x = 0.2$ or a corresponding Fermi wave vector $k_F \simeq 0.67 \text{ \AA}^{-1}$. In Fig. 3 we investigate the temperature dependence of the PG at this doping. The clear gap, persisting all along the antinodal direction at $T = 6 \text{ K}$ (Fig. 3a), gradually becomes less pronounced as temperature increases and completely disappears by $T = 235 \text{ K}$. This behavior is reflected in the symmetrized EDCs at the antinodal k_F (Fig. 3b), which show no discernible trace of a gap at the highest temperature of 235 K. Measurements along the nodal direction (see Supplemental Information C) show that the quasiparticle peak persists even at the highest temperatures, albeit broadened. Low-temperature spectra taken immediately after the temperature-dependent measurements, as shown in Supplemental Information C, exhibit similar features to those observed before the temperature cycle. This rules out that the PG disappears in the data because of aging effects. We thus conclude that the PG closes in the temperature range 150 K – 235 K. Further evidence for the closure of the PG comes from the temperature evolution of the spectral weight W_F at the Fermi surface (see Fig. 3b and Methods for the determination of W_F). At low temperature, the PG suppresses W_F around the antinode ($\theta = \pm 45^\circ$). Raising the temperature, the nodal-antinodal anisotropy gradually reduces and eventually vanishes leaving only a local maximum around $\theta \sim 30^\circ$ where the Fermi arc and its backfolded replica cross.

We remark that the PG reported in Ref. [22] for surface K-doped Sr_2IrO_4 appears to be more fragile than the PG of bulk La-doped $\text{Sr}_{2-x}\text{La}_x\text{IrO}_4$. In the K/ Sr_2IrO_4 system the PG was observed to fully close at a K coverage of $\sim 0.85 \text{ ML}$ corresponding to $k_F \simeq 0.67 \text{ \AA}^{-1}$. Our data show that at the same k_F , the PG clearly remains open in bulk doped samples. Moreover, the temperature boundary of $T^* \simeq 200 \text{ K}$ found here for $x = 0.2$ is significantly higher than the maximal $T^* = 70 \text{ K} - 110 \text{ K}$ at the K/ Sr_2IrO_4 interface observed at a lower doping (coverage of $0.7 \text{ ML} / k_F \simeq 0.655 \text{ \AA}^{-1}$). In addition, surface doped Sr_2IrO_4 shows an apparent d -wave gap, suggesting potential high-temperature surface superconductivity [30, 31]. Our data on bulk doped samples exclude a d -wave gap of similar magnitude and temperature dependence over the entire doping/ k_F range studied in Refs. [30, 31].

The temperature boundary of the PG in bulk electron-

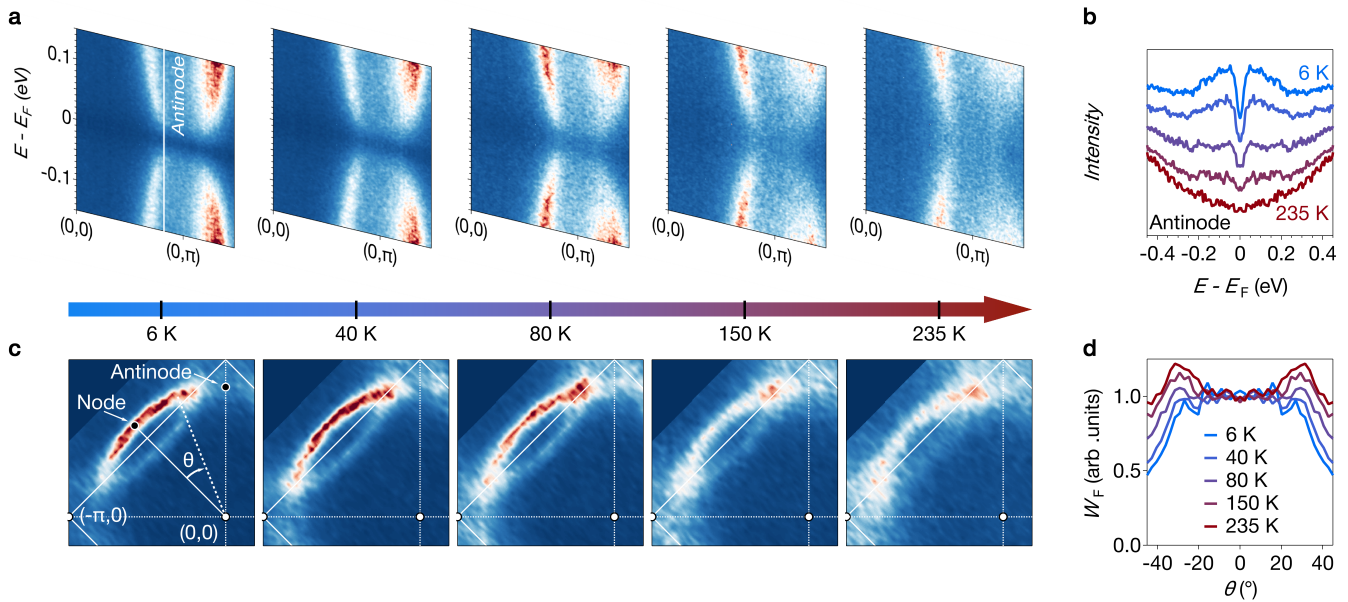


FIG. 3. **Temperature closure of the pseudogap for $x = 0.2$.** **a** Temperature dependence of the symmetrized band dispersion in the antinodal direction. **b** EDCs at the antinode (offset for clarity). **c** Temperature evolution of the Fermi surface. **d** Temperature dependence of the spectral weight W_F along the Fermi surface. The angle θ is defined in panel (c). Data were averaged over $\pm\theta$. See Methods for the procedure used to extract W_F .

doped iridates observed here is strikingly similar to T^* in cuprates [32, 33]. This is intriguing considering the much lower on-site repulsion U and stronger spin-orbit coupling λ_{SOC} in iridates [18, 34, 35]. On the other hand, iridates and cuprates show similar energy scales in the magnetic sector. Magnons in undoped Sr_2IrO_4 disperse up to ~ 205 meV at $(\pi, 0)$ [18], comparable to the ~ 320 meV in La_2CuO_4 [36]. Moreover, spin fluctuations in both iridates [19, 37] and cuprates [38, 39] are known to persist up to high doping. Given these experimental findings, it is compelling to attribute the PG in iridates to short range antiferromagnetic spin fluctuations. In turn, this provides further evidence for the importance of AF correlations for the PG in cuprates, which is also seen in numerical solutions of the Hubbard model [27, 40–44].

We further note a pronounced asymmetry between electron- and hole-doped iridates. A recent study of hole-doped $\text{Sr}_{1.93}\text{K}_{0.07}\text{IrO}_4$ films found a conventional large FS, in sharp contrast to the PG state of $\text{Sr}_{2-x}\text{La}_x\text{IrO}_4$ [45]. This is reminiscent of differences observed in hole- and electron-doped cuprates, although it remains unclear whether the underlying origins are similar. Indeed, both the orbitals involved and the nature of the insulating ground state are different: Cu e_g and O $2p$ orbitals with a large charge-transfer gap for the cuprates, spin-orbitally entangled Ir t_{2g} orbitals with small putative Mott-Hubbard gap in the iridate. Consequently, in cuprates doped holes have a different orbital character than doped electrons [46], while they have different internal degrees of freedom in iridates and thus a different

motion in their local magnetic environment [47].

In summary, our ARPES measurements of highly electron-doped $\text{Sr}_{2-x}\text{La}_x\text{IrO}_4$ crystals reveal a smooth evolution of the electronic structure through the putative critical doping $x^* \simeq 0.16$ identified in recent macroscopic measurements [1]. Within the energy resolution and temperature scale probed by our experiments, there are no signs of a transition from the PG regime with Fermi arcs to a conventional FS, or of an abrupt change in the quasiparticle many-body renormalization over the entire doping range of $x = 0.1 - 0.2$. We can further exclude a Lifshitz transition in this doping range. The origin of the Hall carrier density crossover and the specific heat enhancement reported at $x^* \simeq 0.16$ thus remains deeply mysterious [1]. Future investigations of iridates up to even higher doping levels will undoubtedly provide new insight into the relation of their intriguing PG with transport and specific heat anomalies, and more generally into PG states in the absence of superconductivity.

METHODS

Crystal growth

Single crystals with less than 6% lanthanum content (LD samples) were grown using a conventional flux cooling method, detailed elsewhere [14]. The lanthanum percentage is defined as $N(\text{La})/(N(\text{Sr}) + N(\text{La}))$, and was measured by energy-dispersive X-ray spectroscopy and electron probe X-ray microanalysis. A flux evaporation method was used for crystals with high lanthanum con-

centrations (HD samples). SrCl_2 (Alfa Aesar, anhydrous, 2N_5) flux was combined with SrCO_3 (Sigma Aldrich, 4N), IrO_2 (Alfa Aesar, 3N) and La_2O_3 (Sigma Aldrich, 4N) in ratio $\text{IrO}_2 + 8.5\text{SrCl}_2 + 1.44\text{SrCO}_3 + 0.36\text{La}_2\text{O}_3$. The SrCO_3 was dried at 600°C and La_2O_3 at 1000°C for 24 h. 0.83 g of IrO_2 was used for the successful attempts. All materials were ground in an agate mortar and pestle for twenty minutes and loaded into a 30 mL platinum crucible with a loose platinum lid. The crucible was loaded into a standard box furnace at 700°C , ramped to 1350°C in 3 h and held at 30 h. It was removed at 800°C , and air quenched to room temperature.

The crucible held a mixture of phases, including large ($< 2\text{ mm}$), square platelet samples (perhaps twenty per batch) and iridium metal. Little flux remained in the crucible, and the crystals were removed by soaking in warm water. There were often several morphologies, including triangular-platelet and square-platelet. Interestingly, the square-platelet crystals were consistently above 9% La doping, while the triangular-platelet crystals were less than 6%. The successful method was highly susceptible to synthesis conditions. Variations in starting mass, time baking, crucible volume and temperature could all affect the outcome, preventing crystal growth of high La concentrations. The baking time needed to be long enough for the majority of the flux to evaporate, driving the growth of large crystals. The temperature window of successful growth was small, perhaps twenty degrees Celsius, vital to achieve high doping. Essentially, the intermediate oxidation state of the iridium required for high lanthanum doping is stabilised by temperature and chemical environment. If the temperature is too low, the iridium will not be sufficiently reduced, and if it is too high, the flux will evaporate too quickly, and the iridium will be reduced to metal. Successful reproduction of our method will require fine-tuning individual set-ups to optimise the temperature and starting mass/growth time.

ARPES measurements

Angle-Resolved Photoemission Spectroscopy (ARPES) experiments were performed at the I05 beamline (Diamond Light Source), the BLOCH beamline (Max IV), and the SIS beamline (Swiss Light Source). Samples were cleaved in ultra-high vacuum conditions ($P < 10^{-10}$ mbar) and at low temperatures ($T \simeq 50\text{ K}$ for insulating samples, $T \leq 20\text{ K}$ for conducting samples). Measurements were carried out using photon energies of $h\nu = 68\text{ eV}$ or 100 eV , with an energy resolution ranging from 10 meV to 30 meV , depending on the specific measurement. The Fermi level was calibrated from reference measurements on a polycrystalline Au sample.

Details on data analysis

The Fermi surface maps from undoped and lightly doped samples ($x \leq 0.1$) shown in Fig. 1 are extracted from the

dataset of Ref. [14].

Fermi momenta k_F and scattering rates at the Fermi energy Γ_F , depicted in Fig. 2b,e, were obtained by fitting nodal Momentum Distribution Curves (MDCs) integrated over the range $E = E_F \pm 5\text{ meV}$. The MDCs, extending over the entire Brillouin zone, were modeled using four Lorentzian peaks with a second-order polynomial background, convolved with a Gaussian profile of full width at half maximum $\Delta E/v_F$ where ΔE is the energy resolution and v_F the Fermi velocity. The Fermi velocity v_F in Fig. 2 was obtained from linear fits of the MDC peak dispersion between $E_F - 30\text{ meV}$ and $E_F - 10\text{ meV}$. Where available, the values of k_F , Γ_F , and v_F extracted from both sides of the Γ points were averaged.

To determine the pseudogap area as a function of the angle θ in Fig. 2c, we first removed a second-order polynomial background defined far from E_F (typically from $E - E_F = -0.3\text{ eV}$ to $E - E_F = -0.05\text{ eV}$) to EDCs averaged over the range $k_F \pm 0.015\text{ \AA}^{-1}$ and measured at a given angle θ . The background-subtracted symmetrized EDCs relative to E_F were fitted with a Gaussian profile, the area of which were averaged for $\pm\theta$ and define the pseudogap area.

The spectral weight at the Fermi level W_F shown in Fig. 2b was obtained by averaging the measured intensity in the range $E_F \pm 10\text{ meV}$ and $k_F \pm 0.015\text{ \AA}^{-1}$ at $\pm\theta$ for $\theta \in [-45^\circ, 45^\circ]$. For each temperature T , this quantity was normalised by the average nodal spectral weight $W_F(\theta \in [0^\circ, \pm 5^\circ], T)$.

ACKNOWLEDGMENTS

We thank K. Wohlfeld for discussion. This work was supported by the Swiss National Science Foundation grants 146995, 165791, 184998. We acknowledge Diamond Light Source for time on Beamline I05 under Proposals SI10348, SI12404, SI17381. We acknowledge MAX IV Laboratory for time on Beamline Bloch under Proposal No. 20220192 and 20231600. Research conducted at MAX IV, a Swedish national user facility, is supported by the Swedish Research Council under Contract No. 2018-07152, the Swedish Governmental Agency for Innovation Systems under Contract No. 2018-04969, and Formas under Contract No. 2019-0249 We acknowledge the Paul Scherrer Institut, Villigen, Switzerland for provision of synchrotron radiation beamtime at the SIS beamline of the SLS.

* yann.alexanian@unige.ch

[1] Y.-T. Hsu, A. Rydh, M. Berben, C. Duffy, A. de la Torre, R. S. Perry, and N. E. Hussey, Carrier density crossover

- and quasiparticle mass enhancement in a doped 5d mott insulator, *Nature Physics* **20**, 1596 (2024).
- [2] M. R. Norman, H. Ding, M. Randeria, J. C. Campuzano, T. Yokoya, T. Takeuchi, T. Takahashi, T. Mochiku, K. Kadowaki, P. Guptasarma, and D. G. Hinks, Destruction of the fermi surface in underdoped high-*t_c* superconductors, *Nature* **392**, 157 (1998).
 - [3] K. M. Shen, F. Ronning, D. H. Lu, F. Baumberger, N. J. C. Ingle, W. S. Lee, W. Meevasana, Y. Kohsaka, M. Azuma, M. Takano, H. Takagi, and Z.-X. Shen, Nodal Quasiparticles and Antinodal Charge Ordering in $\text{Ca}_2 - x\text{Na}_x\text{CuO}_2\text{Cl}_2$, *Science* **307**, 901 (2005).
 - [4] P. A. Lee, N. Nagaosa, and X.-G. Wen, Doping a mott insulator: Physics of high-temperature superconductivity, *Reviews of Modern Physics* **78**, 17 (2006).
 - [5] M. Civelli, M. Capone, S. S. Kancharla, O. Parcollet, and G. Kotliar, Dynamical breakup of the fermi surface in a doped mott insulator, *Physical Review Letters* **95** (2005).
 - [6] G. Sordi, A. Amaricci, and M. J. Rozenberg, Metal-insulator transitions in the periodic anderson model, *Physical Review Letters* **99** (2007).
 - [7] C. Proust and L. Taillefer, The remarkable underlying ground states of cuprate superconductors, *Annual Review of Condensed Matter Physics* **10**, 409 (2019).
 - [8] S. Badoux, W. Tabis, F. Laliberté, G. Grissonnanche, B. Vignolle, D. Vignolles, J. Béard, D. A. Bonn, W. N. Hardy, R. Liang, N. Doiron-Leyraud, L. Taillefer, and C. Proust, Change of carrier density at the pseudogap critical point of a cuprate superconductor, *Nature* **531**, 210 (2016).
 - [9] C. Putzke, S. Benhabib, W. Tabis, J. Ayres, Z. Wang, L. Malone, S. Licciardello, J. Lu, T. Kondo, T. Takeuchi, N. E. Hussey, J. R. Cooper, and A. Carrington, Reduced hall carrier density in the overdoped strange metal regime of cuprate superconductors, *Nature Physics* **17**, 826 (2021).
 - [10] B. J. Kim, H. Jin, S. J. Moon, J.-Y. Kim, B.-G. Park, C. S. Leem, J. Yu, T. W. Noh, C. Kim, S.-J. Oh, J.-H. Park, V. Durairaj, G. Cao, and E. Rotenberg, Novel $J_{\text{eff}} = 1/2$ mott state induced by relativistic spin-orbit coupling in Sr_2IrO_4 , *Physical Review Letters* **101**, 076402 (2008).
 - [11] B. J. Kim, H. Ohsumi, T. Komesu, S. Sakai, T. Morita, H. Takagi, and T. Arima, Phase-Sensitive Observation of a Spin-Orbital Mott State in Sr_2IrO_4 , *Science* **323**, 1329 (2009).
 - [12] H. Jin, H. Jeong, T. Ozaki, and J. Yu, Anisotropic exchange interactions of spin-orbit-integrated states in Sr_2IrO_4 , *Physical Review B* **80**, 075112 (2009).
 - [13] D. Choi, C. Yue, D. Azoury, Z. Porter, J. Chen, F. Petocchi, E. Baldini, B. Lv, M. Mogi, Y. Su, S. D. Wilson, M. Eckstein, P. Werner, and N. Gedik, Light-induced insulator-metal transition in Sr_2IrO_4 reveals the nature of the insulating ground state, *Proceedings of the National Academy of Sciences* **121**, e2323013121 (2024).
 - [14] A. de la Torre, S. McKeown Walker, F. Bruno, S. Riccó, Z. Wang, I. Gutierrez Lezama, G. Scheerer, G. Girit, D. Jaccard, C. Berthod, T. Kim, M. Hoesch, E. Hunter, R. Perry, A. Tamai, and F. Baumberger, Collapse of the Mott Gap and Emergence of a Nodal Liquid in Lightly Doped Sr_2IrO_4 , *Physical Review Letters* **115**, 176402 (2015).
 - [15] V. Brouet, J. Mansart, L. Perfetti, C. Piovera, I. Vobornik, P. Le Fèvre, F. Bertran, S. C. Riggs, M. C. Shapiro, P. Giraldo-Gallo, and I. R. Fisher, Transfer of spectral weight across the gap of Sr_2IrO_4 induced by la doping, *Physical Review B* **92**, 081117(R) (2015).
 - [16] S. Peng, C. Lane, Y. Hu, M. Guo, X. Chen, Z. Sun, M. Hashimoto, D. Lu, Z.-X. Shen, T. Wu, X. Chen, R. S. Markiewicz, Y. Wang, A. Bansil, S. D. Wilson, and J. He, Electronic nature of the pseudogap in electron-doped Sr_2IrO_4 , *npj Quantum Materials* **7**, 58 (2022).
 - [17] K. Wang, N. Bachar, J. Teyssier, W. Luo, C. W. Rischau, G. Scheerer, A. de la Torre, R. S. Perry, F. Baumberger, and D. van der Marel, Mott transition and collective charge pinning in electron doped Sr_2IrO_4 , *Physical Review B* **98**, 045107 (2018).
 - [18] J. Kim, D. Casa, M. H. Upton, T. Gog, Y.-J. Kim, J. F. Mitchell, M. van Veenendaal, M. Daghofer, J. van den Brink, G. Khaliullin, and B. J. Kim, Magnetic excitation spectra of Sr_2IrO_4 probed by resonant inelastic x-ray scattering: Establishing links to cuprate superconductors, *Physical Review Letters* **108**, 177003 (2012).
 - [19] D. Pincini, J. G. Vale, C. Donnerer, A. de la Torre, E. C. Hunter, R. Perry, M. Moretti Sala, F. Baumberger, and D. F. McMorrow, Anisotropic exchange and spin-wave damping in pure and electron-doped Sr_2IrO_4 , *Physical Review B* **96**, 075162 (2017).
 - [20] J. Saylor, L. Takacs, C. Hohenemser, J. I. Budnick, and B. Chamberland, Néel temperature of stoichiometric La_2CuO_4 , *Physical Review B* **40**, 6854 (1989).
 - [21] S. M. Hayden, G. Aeppli, R. Osborn, A. D. Taylor, T. G. Perring, S.-W. Cheong, and Z. Fisk, High-energy spin waves in La_2CuO_4 , *Physical Review Letters* **67**, 3622 (1991).
 - [22] Y. K. Kim, O. Krupin, J. D. Denlinger, A. Bostwick, E. Rotenberg, Q. Zhao, J. F. Mitchell, J. W. Allen, and B. J. Kim, Fermi arcs in a doped pseudospin-1/2 Heisenberg antiferromagnet, *Science* **345**, 187 (2014).
 - [23] M. K. Crawford, M. A. Subramanian, R. L. Harlow, J. A. Fernandez-Baca, Z. R. Wang, and D. C. Johnston, Structural and magnetic studies of Sr_2IrO_4 , *Physical Review B* **49**, 9198 (1994).
 - [24] F. Ye, S. Chi, B. C. Chakoumakos, J. A. Fernandez-Baca, T. Qi, and G. Cao, Magnetic and crystal structures of Sr_2IrO_4 : A neutron diffraction study, *Physical Review B* **87**, 140406(R) (2013).
 - [25] K. M. Shen, F. Ronning, D. H. Lu, W. S. Lee, N. J. C. Ingle, W. Meevasana, F. Baumberger, A. Damascelli, N. P. Armitage, L. L. Miller, Y. Kohsaka, M. Azuma, M. Takano, H. Takagi, and Z.-X. Shen, Missing quasiparticles and the chemical potential puzzle in the doping evolution of the cuprate superconductors, *Physical Review Letters* **93**, 267002 (2004).
 - [26] D. Fournier, G. Levy, Y. Penec, J. L. McChesney, A. Bostwick, E. Rotenberg, R. Liang, W. N. Hardy, D. A. Bonn, I. S. Elfimov, and A. Damascelli, Loss of nodal quasiparticle integrity in underdoped $\text{yba}_2\text{cu}_3\text{o}_6+x$, *Nature Physics* **6**, 905 (2010).
 - [27] A. Moutenet, A. Georges, and M. Ferrero, Pseudogap and electronic structure of electron-doped Sr_2IrO_4 , *Physical Review B* **97**, 155109 (2018).
 - [28] W. S. Lee, I. M. Vishik, K. Tanaka, D. H. Lu, T. Sasagawa, N. Nagaosa, T. P. Devereaux, Z. Hussain, and Z. X. Shen, Abrupt onset of a second energy gap at the superconducting transition of underdoped $\text{bi}2212$,

- Nature* **450**, 81 (2007).
- [29] S. McKeown Walker, F. Y. Bruno, Z. Wang, A. de la Torre, S. Riccò, A. Tamai, T. K. Kim, M. Hoesch, M. Shi, M. S. Bahramy, P. D. C. King, and F. Baumberger, Carrier-Density Control of the SrTiO₃ (001) Surface 2D Electron Gas studied by ARPES, *Advanced Materials* **27**, 3894 (2015).
- [30] Y. K. Kim, N. H. Sung, J. D. Denlinger, and B. J. Kim, Observation of a d-wave gap in electron-doped Sr₂IrO₄, *Nature Physics* **12**, 37 (2015).
- [31] Y. Yan, M. Ren, H. Xu, B. Xie, R. Tao, H. Choi, N. Lee, Y. Choi, T. Zhang, and D. Feng, Electron-doped Sr₂IrO₄: An analogue of hole-doped cuprate superconductors demonstrated by scanning tunneling microscopy, *Physical Review X* **5**, 041018 (2015).
- [32] T. Yoshida, M. Hashimoto, S. Ideta, A. Fujimori, K. Tanaka, N. Mannella, Z. Hussain, Z.-X. Shen, M. Kubota, K. Ono, S. Komiya, Y. Ando, H. Eisaki, and S. Uchida, Universal versus material-dependent two-gap behaviors of the high-*t_c* cuprate superconductors: Angle-resolved photoemission study of La_{2-x}Sr_xCuO₄, *Physical Review Letters* **103**, 037004 (2009).
- [33] O. Cyr-Choinière, R. Daou, F. Laliberté, C. Collignon, S. Badoux, D. LeBoeuf, J. Chang, B. J. Ramshaw, D. A. Bonn, W. N. Hardy, R. Liang, J.-Q. Yan, J.-G. Cheng, J.-S. Zhou, J. B. Goodenough, S. Pyon, T. Takayama, H. Takagi, N. Doiron-Leyraud, and L. Taillefer, Pseudogap temperature T^* of cuprate superconductors from the nernst effect, *Physical Review B* **97**, 064502 (2018).
- [34] S. J. Moon, H. Jin, W. S. Choi, J. S. Lee, S. S. A. Seo, J. Yu, G. Cao, T. W. Noh, and Y. S. Lee, Temperature dependence of the electronic structure of the $J_{\text{eff}} = 1/2$ mott insulator Sr₂IrO₄ studied by optical spectroscopy, *Physical Review B* **80**, 195110 (2009).
- [35] Q. Wang, Y. Cao, J. A. Waugh, S. R. Park, T. F. Qi, O. B. Korneta, G. Cao, and D. S. Dessau, Dimensionality-controlled mott transition and correlation effects in single-layer and bilayer perovskite iridates, *Physical Review B* **87**, 245109 (2013).
- [36] R. Coldea, S. M. Hayden, G. Aeppli, T. G. Perring, C. D. Frost, T. E. Mason, S.-W. Cheong, and Z. Fisk, Spin waves and electronic interactions in la₂cuo₄, *Phys. Rev. Lett.* **86**, 5377 (2001).
- [37] H. Gretarsson, N. Sung, J. Porras, J. Bertinshaw, C. Dietl, J. A. Bruin, A. Bangura, Y. Kim, R. Dinnebier, J. Kim, A. Al-Zein, M. Moretti Sala, M. Krisch, M. Le Tacon, B. Keimer, and B. Kim, Persistent paramagnons deep in the metallic phase of Sr_{2-x}La_xIrO₄, *Physical Review Letters* **117**, 107001 (2016).
- [38] B. Keimer, N. Belk, R. J. Birgeneau, A. Cassanho, C. Y. Chen, M. Greven, M. A. Kastner, A. Aharony, Y. Endoh, R. W. Erwin, and G. Shirane, Magnetic excitations in pure, lightly doped, and weakly metallic La₂CuO₄, *Physical Review B* **46**, 14034 (1992).
- [39] G. Drachuck, E. Razzoli, G. Bazalitski, A. Kanigel, C. Niedermayer, M. Shi, and A. Keren, Comprehensive study of the spin-charge interplay in antiferromagnetic La_{2-x}Sr_xCuO₄, *Nature Communications* **5**, 3390 (2014).
- [40] B. Kyung, S. S. Kancharla, D. Sénéchal, A.-M. S. Tremblay, M. Civelli, and G. Kotliar, Pseudogap induced by short-range spin correlations in a doped mott insulator, *Physical Review B* **73**, 165114 (2006).
- [41] O. Gunnarsson, T. Schäfer, J. LeBlanc, E. Gull, J. Merino, G. Sangiovanni, G. Rohringer, and A. Toschi, Fluctuation diagnostics of the electron self-energy: Origin of the pseudogap physics, *Physical Review Letters* **114**, 236402 (2015).
- [42] W. Wu, M. Ferrero, A. Georges, and E. Kozik, Controlling feynman diagrammatic expansions: Physical nature of the pseudogap in the two-dimensional hubbard model, *Physical Review B* **96**, 041105(R) (2017).
- [43] H. Wang, S.-L. Yu, and J.-X. Li, Fermi arcs, pseudogap, and collective excitations in doped Sr₂IrO₄: A generalized fluctuation exchange study, *Physical Review B* **91**, 165138 (2015).
- [44] F. Šimkovic, R. Rossi, A. Georges, and M. Ferrero, Origin and fate of the pseudogap in the doped Hubbard model, *Science* **385**, eade9194 (2024).
- [45] J. N. Nelson, C. T. Parzyck, B. D. Faeth, J. K. Kawasaki, D. G. Schlom, and K. M. Shen, Mott gap collapse in lightly hole-doped Sr_{2-x}K_xIrO₄, *Nature Communications* **11**, 2597 (2020).
- [46] N. P. Armitage, P. Fournier, and R. L. Greene, Progress and perspectives on electron-doped cuprates, *Rev. Mod. Phys.* **82**, 2421 (2010).
- [47] E. M. Pärshcke, K. Wohlfeld, K. Foyevtsova, and J. van den Brink, Correlation induced electron-hole asymmetry in quasi- two-dimensional iridates, *Nature Communications* **8**, 686 (2017).

Supplementary Information for "Fermi surface and pseudogap in highly doped Sr_2IrO_4 "

Y. Alexanian,^{1,*} A. de la Torre,² S. McKweon Walker,³ M. Straub,¹ G. Gatti,¹ A. Hunter,¹ S. Mandloi,¹ E. Cappelli,¹ S. Riccò,¹ F. Y. Bruno,⁴ M. Radovic,⁵ N. C. Plumb,⁵ M. Shi,⁵ J. Osiecki,⁶ C. Polley,⁶ T. K. Kim,⁷ P. Dudin,^{7,8} M. Hoesch,⁹ R. S. Perry,^{10,11} A. Tamai,¹ and F. Baumberger^{1,5}

¹*Department of Quantum Matter Physics, University of Geneva,
24 Quai Ernest-Ansermet, CH-1211, Geneva, Switzerland*

²*Department of Physics, Brown University, Providence, Rhode Island 02912, USA*

³*Laboratory of Advanced Technology, University of Geneva,
24 Quai Ernest-Ansermet, CH-1211, Geneva, Switzerland*

⁴*GFMC, Departamento de Física de Materiales, Universidad Complutense de Madrid, 28040 Madrid, Spain*

⁵*Swiss Light Source, Paul Scherrer Institut, CH-5232 Villigen PSI, Switzerland*

⁶*MAX IV Laboratory, Lund University, SE-211 00 Lund, Sweden*

⁷*Diamond Light Source, Harwell Campus, Didcot, OX11 0DE, United Kingdom*

⁸*Synchrotron SOLEIL, L'Orme des Merisiers, Saint Aubin-BP 48, 91192 Gif sur Yvette Cedex, France*

⁹*Deutsches Elektronen-Synchrotron DESY, Notkestraße 85, 22607 Hamburg, Germany*

¹⁰*ISIS Pulsed Neutron and Muon Source, STFC Rutherford Appleton Laboratory,
Harwell Campus, Didcot, Oxon OX11 0QX, United Kingdom*

¹¹*London Centre for Nanotechnology and Department of Physics and Astronomy,
University College London, London WC1E 6BT, United Kingdom*

(Dated: November 28, 2024)

A. SAMPLE CHARACTERIZATION AND DOPING DEPENDENCE

In Fig. S1, we present the evolution of the ARPES spectra of $\text{Sr}_{2-x}\text{La}_x\text{IrO}_4$ as a function of the ARPES spot position in one of our HD samples, which exhibits inhomogeneous chemical doping x . Spectra in the nodal direction measured at several points spaced by $30\ \mu\text{m}$ (see Fig. S1a) are shown in Fig. S1b. Significant changes in the electronic structure near the Fermi energy are observed: the two branches around $(\pi/2, \pi/2)$, forming the lenses of the Fermi surface, are indistinguishable near the sample edge but become clearly visible towards its center. This evolution correlates with variations in the lanthanum concentration x along the line, as measured by energy-dispersive X-ray spectroscopy (EDX), and shown in Fig. S1c. Interestingly, we found that the Fermi momentum k_F (extracted from MDCs at $E = E_F$) increases linearly with the chemical doping value x (Fig. S1d). Although the chemical doping x cannot be directly related to electron doping (see main text), its evolution in a single type of sample reflects changes in electron doping. Finally, note that this spatial variation of x is typical for our HD samples, whereas LD samples exhibit a more homogeneous doping distribution.

B. ANGULAR DEPENDENCE OF THE PSEUDOGAP

In Fig. S2 we provide additional details on the determination of the angular dependence of the pseudogap shown in Fig. 2c of the main text. First, we fitted a second-order polynomial background $B(E - E_F)$ in the energy interval $-0.3\ \text{eV} \leq E - E_F \leq -0.05\ \text{eV}$ of the EDCs measured at k_F for various angles θ (each EDC corresponds to a color dot in Fig. 2c). We then removed the background of the EDCs and fitted the symmetrized remaining signal in the energy range $-0.05\ \text{eV} \leq E - E_F \leq 0.05\ \text{eV}$ with a Gaussian function defined as:

$$G(E - E_F) = \frac{A}{2\gamma\sqrt{\pi/\ln(16)}} \exp\left(-\left(\frac{E - E_F}{2\gamma}\right)^2 \ln(16)\right). \quad (\text{S1})$$

Examples of the EDCs and their total fits $B(E - E_F) + G(E - E_F)$ are shown in Fig. S2a for $x = 0.1$ and Fig. S2b for $x = 0.2$. The spectral weight suppression in the PG, shown in Fig. 2c of the main text, is defined as the area A . Figs. S2c,d,e show the area A together with the gap width γ , and the gap amplitude A/γ . Interestingly, our fits also indicate that it is the gap amplitude, rather than the gap width, that decreases as the node is approached. Lastly, note the presence of a local maximum (and corresponding local minimum) in the gap area (gap width) around $\pm 30^\circ$, where the primitive and backfolded bands cross.

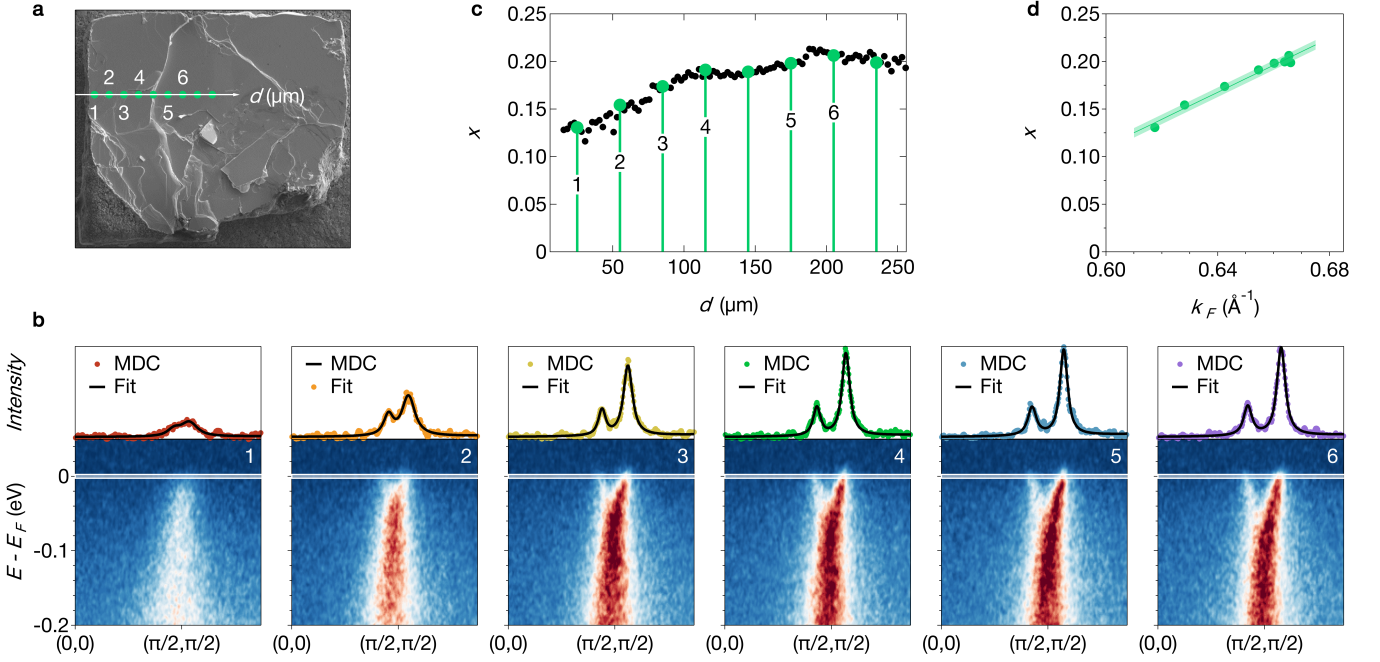


FIG. S1. **Spatial dependence of the ARPES spectra measured in an HD sample.** **a** Scanning electron microscope image of a cleaved sample. The green dots represent the position and size of the ARPES spots at different measurement points. The spot size was approximately $10\ \mu\text{m}$, and the points were spaced by $30\ \mu\text{m}$ along a line (in white). **b** ARPES cuts and MDCs at the Fermi energy (integrated over the range $E = E_F \pm 25\ \text{meV}$) along the nodal direction measured at different positions on the sample, as shown in panel (a). MDCs are fitted with two Lorentzian peaks and a second-order polynomial background convolved with a Gaussian profile of full width at half maximum determined by the energy resolution. **c** EDX characterization of the doping value x along the line of the ARPES measurements, see panel (a). Green lines and dots correspond to the positions of the ARPES measurement points. **d** Fermi momentum k_F extracted from the MDCs as a function of the chemical doping value x obtained from EDX measurements. The green line is a linear fit to the data.

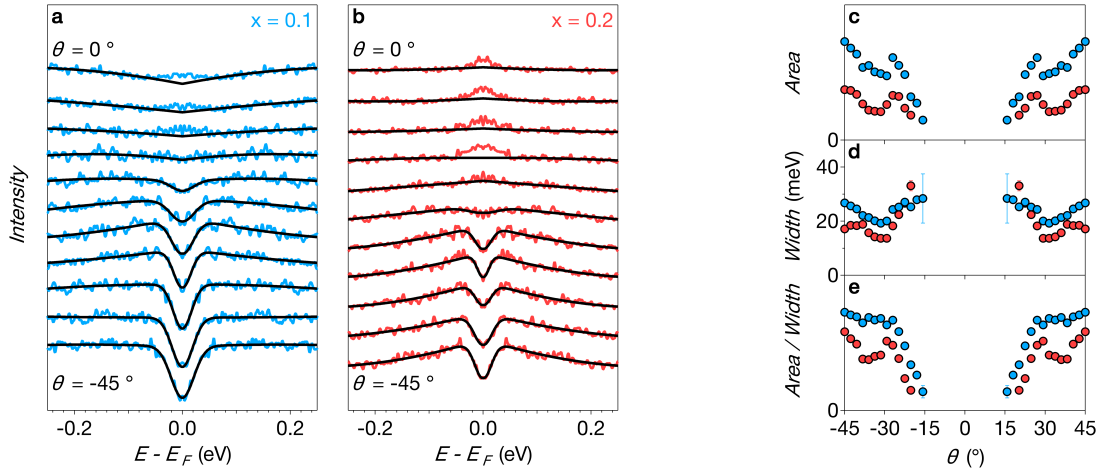


FIG. S2. **Angular dependence of the $\text{Sr}_{2-x}\text{La}_x\text{IrO}_4$ pseudogap for $x = 0.1$ and $x = 0.2$.** **a,b** Fits of the symmetrized EDCs (with respect to E_F) measured at k_F with an angle θ compared to the nodal direction. The fitting procedure is described in the supplementary text. **c** Pseudogap area A , **d** pseudogap width γ , and **e** pseudogap amplitude A/γ as a function of the angle θ compared to the nodal direction. Values obtained for angles $+\theta$ and $-\theta$ were averaged.

C. COMPLEMENT ON THE TEMPERATURE DEPENDENCE

In Fig. S3 we present temperature-dependent measurements of the electronic structure of $\text{Sr}_{1.8}\text{La}_{0.2}\text{IrO}_4$ along the nodal direction. Symmetrized cuts from $T = 6\text{ K}$ to $T = 235\text{ K}$ (see Fig. S3a) reveal the absence of any gap within this temperature range, in stark contrast to the temperature-dependent pseudogap observed in the antinodal direction (see Fig. 3a of main text). Moreover, the nodal EDCs at different temperature, shown in Fig. S3b, demonstrate that the sharp quasiparticle peak visible at $T = 6\text{ K}$ broadens with increasing temperature but remains present up to the highest temperature measured. Notably, we observe no significant change when the pseudogap closes (between $T = 150\text{ K}$ and $T = 235\text{ K}$).

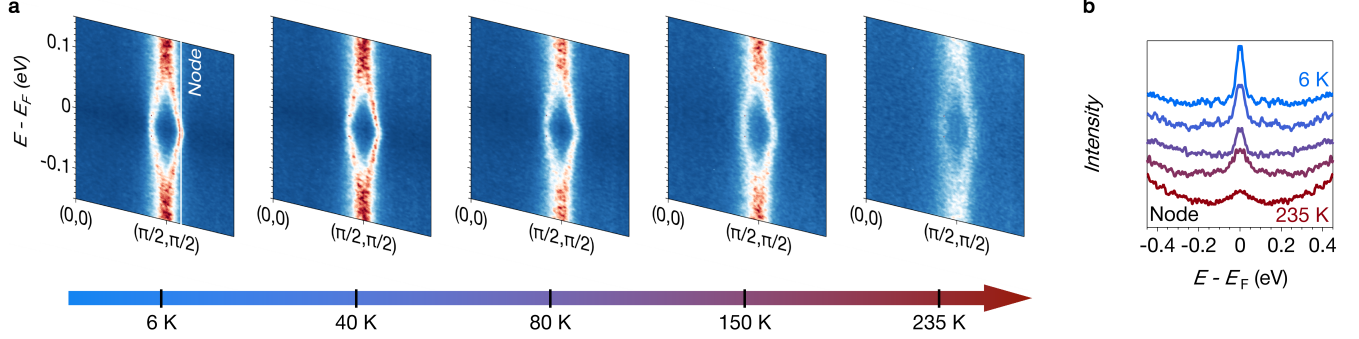


FIG. S3. **Temperature dependence of nodal ARPES spectra in $\text{Sr}_{1.8}\text{La}_{0.2}\text{IrO}_4$.** **a** Temperature dependence of the symmetrized band dispersion in the nodal direction. The node position is indicated by the white line. **b** EDCs at the node, shifted by a different constant intensity for each temperature.

Low-temperature measurements ($T = 20\text{ K}$) taken after the complete temperature cycle from $T = 6\text{ K}$ to $T = 235\text{ K}$ are shown in Fig. S4. Symmetrized cuts along both the nodal and antinodal directions (Figs. S4a,b) as well as the Fermi surface (Fig. S4c) are similar to those obtained at low temperature before the cycle (see Figs. 3 and S3). Most importantly, a pseudogap remains evident at the antinode, while no gap is observed at the node, ruling out any aging effect as an explanation for the pseudogap closure in our data.

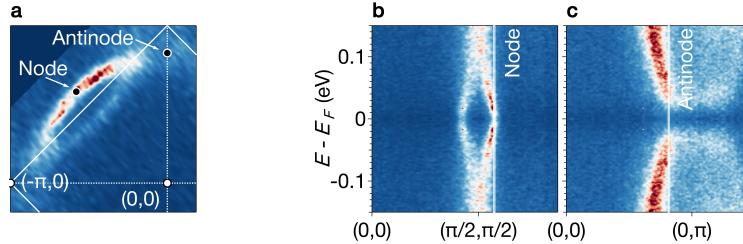


FIG. S4. **Low-temperature measurements of $\text{Sr}_{1.8}\text{La}_{0.2}\text{IrO}_4$ after a complete temperature cycle.** **a,b** Symmetrized cuts along the nodal and antinodal directions, respectively. **c** Fermi surface.